RAL-TR –2004-027

A PROTOTYPE 2-D GMSD BASED IMAGING DETECTOR FOR X-RAYS

J.E.Bateman, G.E.Derbyshire, D.M.Duxbury, A.S.Marsh, N.J.Rhodes,
E.M.Schooneveld, E.J.Spill and R.Stephenson

Rutherford Appleton Laboratory, Chilton, Didcot, Oxon, OX11 0QX, U.K.

19th November 2004

Abstract

The development and testing of a 2-D prototype detector based on a gas microstrip detector (GMSD) is reported. The second spatial co-ordinate is obtained by utilising a plane of orthogonal wires as pick up electrodes. The detector is operated with the wire plane at such a potential so as not to induce any gain around the wires. This means that the high tolerances normally associated with wire planes in Multi-Wire Proportional Counters are not necessary, making the manufacture and repair of such a device relatively easier. The detector comprises of 48 individually instrumented channels in both X (GMSD strips) and Y (transverse wire plane). A specially designed encoding module has been constructed which feeds digital addresses for each event to the ISIS data taking electronics system (DAE). An intrinsic detector resolution of ~0.5mm FWHM has been measured for both dimensions which is degraded slightly by the digital resolution for the overall system. This readout method is shown to be very tolerant of a poor signal to noise ratio in the readout channels (unlike traditional analogue wire chamber readout systems) and permits the operation of the GMSD at moderate avalanche gains (~1000). This helps to maximise the rate and lifetime performance of the detector as well as permitting data capture rates in the MHz range.

1. Introduction

Detectors for ionising radiation based on gas counters come in many forms and play an important role in both photon and particle detection.

Key science areas in materials development within the UK demand large x-ray and neutron sensitive detectors with two-dimensional (2-D) readout to operate on Diamond and on ISIS target station 2. These include: a 2-D detector for Diamond beam line I22 to perform dynamic, non-crystalline diffraction on biological and manmade polymer samples; a 2-D detector for SRS beam line 6.2 to complement the existing 1-D SAXS/WAXS systems, and on ISIS both the single crystal (SX) and reflectometry instruments need 200mm x 200mm 2-D detectors. This report deals specifically with the x-ray imaging applications. The extension of the technique to neutron applications is described elsewhere [1].

Imaging gas counters based on Multi-Wire Proportional Counter (MWPC) technology have a long history of successful application to x-ray diffraction [2-8]. Their properties of low noise, high detective quantum efficiency and the large dynamic range of counting detectors have continued to make gas detectors attractive for application on Synchrotron Radiation (SR) beam lines.

We report the successful testing of a small prototype two dimensional gas microstrip detector of dimensions ~50×50mm capable of MHz readout rates. Several other institutions have made 2-D imaging devices based on GMSDs utilising various methods for obtaining the second dimension. One approach is to use back pads on the GMSD structure [9-11]. Another approach is to modify the GMSD structure [12]. We have followed the approach of Budtz-Jorgensen [13] in using wire plane close to the plate surface to pick up the second dimension.

2. The 2-D GMSD Detector

2.1 Fast 2-D Readout of GMSDs

The GMSD is intrinsically a 1-D device and lends itself to very fast operation with channel-by-channel readout using high density, low noise electronics, as has been demonstrated in x-ray applications such as ref [14]. However, the applications discussed above demand full 2-D readout. This has been achieved in various ways (as referenced above), however in the very high rates of Synchrotron beams, the long-standing (and successful) analogue methods tend to reach their limits well below the MHz capability demanded. The performance and limitations of channel-by channel readout in the 1-D case has been explored at RAL in practical application to x-ray diffraction and neutron beams in parallel with Monte Carlo modelling studies [14-17]. The results of these studies can be summed up as follows:

- In spite of considerable spreading (by diffusion and fast electron range) of the primary signal, the spatial resolution is essentially governed by the strip width (i.e SD (sigma) ≈ W /√12, where SD is the standard deviation and W is the strip width). Because of beam/sample sizes this means that the spatial resolutions of ~0.5mm FWHM attainable by this technique are appropriate for many applications.

- This resolution is very insensitive to the signal to noise ratio in the readout amplifier enabling low gains (~1000 for keV x-rays) to be used in the GMSD.

- The resulting low gain/signal size optimises the rate capability and the lifetime of the detector – important in the Synchrotron environment.

- The main demerit of this readout approach is that it puts a high demand on the uniformity of response of the readout electronics. This is typically a few % and the channel sharing effects have been shown by the MC model to amplify this differential non-linearity by factors of up to two (depending on the detailed design).

- A final drawback of the method is that, because of the signal sharing between channels precise pulse height information (i.e. x-ray energy) is not available. Fortunately in many beam applications this is not a critical requirement.

The purpose of the prototype detector described in this report is to explore the possibility of generalising the channel-by-channel readout method to achieve full 2-D imaging capability. While the need to correlate the X (anode) signals with the Y (orthogonal wire plane) signals forces the readout to be global (and therefore more rate-limiting than the 1-D case), the occupancy time (i.e. the intrinsic length of the x-ray pulse of ~200ns) is applied to only one discriminator circuit at a time so that the correlating and coding electronics can, in principle, perform considerably faster (at MHz rates).

In order to achieve pick-up of the GMSD induction pulse in the direction orthogonal to the anodes (Y) a wire plane of 1mm pitch was set close to the active plate surface at a distance of less than one anode pitch. This method was chosen for several reasons:

- The poor mechanical properties of the semi-insulating S8900 glass (essential for stable, long term operation) precluded using patterned Y electrodes on the rear face since the plate thickness would have to be ≈0.3mm and experience has shown that this is too thin for adequate mechanical strength.

- The low wire capacitance (compared with electrodes on the glass) considerably eases the demands on the Y preamplifiers.

- The wires are robust (0.1mm diameter) and held at the equilibrium potential of the site above the plate so that the demands of tolerance in positioning and tension are greatly reduced from those of the typical Multi-Wire Proportional Counter.

2.2 Detailed design

Figure 1 shows a schematic cross-section of the prototype 2-D detector. The S8900 glass plate is glued to a printed circuit board, and the wire plane for the second co-ordinate is mounted from four spacers at the glass edges some 250µm away from the plate surface. A thin (5µm) aluminium drift plane is mounted 6.1mm from the glass surface to form the x-ray conversion volume. The detector is a legacy from a particle physics project [18] having an anode width of 10µm, a cathode width of 90µm and a pitch of 300µm, resulting in the pitch and the conversion volume being less than ideal for x-ray detection. The wire plane is constructed from gold plated tungsten wires of 100µm diameter, with 48 wires on a pitch of 1mm. The anodes of the glass plate are bussed together in groups of four in order to approximately match the wire plane pitch (giving a pixel size of 1.2mm by 1mm). 48 groups of anodes are used which gives us an active area of 57.6mm in X by 48mm in Y.

The GMSD is typically run with the readout anodes at earth, the plate cathodes at -560V and the drift plane held constant at –2kV. The wire plane is held close to the equipotential voltage between drift and plate, therefore ensuring that the Y wire plane does not influence the gas gain. This has the advantage that the wire plane can then be made without the high tolerances normally associated with wire-based detectors. The structure of figure 1 is housed in a gas tight enclosure with a thin aluminised mylar window above the drift electrode to permit entry of the x-rays. Gas ports and electrical sockets are provided for interface to the readout system. For the present limited tests a gas filling of argon + 25% isobutane was used. For serious long term use the isobutane would be replaced with dimethylether [19].

2.3 Operating Characteristics

The initial testing of the detector was conducted using the typical charge preamplifier/main amplifier/pulse height analyser chain. The x-rays can be used to calibrate the gas gain in the usual way and figure 2 shows the typical gas counter gain curve (gain versus cathode voltage, V_C). It should be stressed that the limit shown in the figure is not the spark limit of the detector. In order for the detector to operate successfully, the signal size induced on the Y wires must be large enough to generate an adequate signal to noise ratio in any Y readout channel. In practice only 14% of the anode signal is induced on any given Y wire. Variation of the wire plane voltage (V_W) produces the useful gas gain (figure 3), but in practice the wire plane is set close to the cathode voltage.

2.4 Electronic readout

The 48 channels in X and Y are individually instrumented with preamplifier, post amplifiers and discriminators as shown schematically in figure 4. The preamplifiers used are 16 channels fast charge amplifiers which have been developed elsewhere [18]. The pulse shaping amplifier was specifically designed to plug into the preamp and is described in [20]. These can be seen in the photograph in figure 5. Figure 6 shows typical pulses from both X and Y for ^{55}Fe x-rays. NIM based Lecroy 612 post amplifiers increase the signal size further before the signals are passed to NE 4684 NIM based discriminators. From here the digital signal is then passed to an in-house built encoding and combining module, which is described in detail in Appendix 1. This module determines the validity of the events, addresses the events, combines the data and sends it to the ISIS data taking electronics (DAE), which has been described elsewhere [21]. The module takes its master trigger from the anode signal and determines if it is a valid event. This is done using an EPROM, which is programmed to accept either single or double (adjacent) channel hits. The EPROM then looks for events on the other 47 channels to veto out any ghost hits. The event is then addressed as a six bit word (dual hits are assigned to the least significant bit). This is repeated for Y, and the module then combines the two readout channels by forming a coincidence between the synchronised X and Y pulses. The x-ray event address is then sent to the DAE. The data capture efficiency has been measured to be greater than 90%.

3. System performance

3.1 Imaging

The detector is usually used with a flowing gas mixture, but was sealed off for use close to the DAE electronics, and was re-gassed on a daily basis. Figure 7 shows the data obtained, when a mask made from copper tape with letters 18mm high and transmission slots of 3-3.5mm was placed on the front window of the chamber and illuminated with 5.9keV x-rays.

In order to measure the intrinsic resolution (unlimited by the digital readout) of the detector, a 0.5mm collimated slit beam of 5.9keV x-rays was set up and scanned across two consecutive pixels in X and two adjacent wires in Y. The X distribution, shown in figure 8, was obtained by summing in Y to produce an X histogram for each scan position. A series of such X scans were obtained. Each distribution was normalised to its centroid and all the distributions summed. This process demonstrates the intrinsic detector resolution with a statistically enhanced digital resolution. The procedure was repeated for Y and the results are shown in figure 9. Gaussian fits to these figures yield a sigma of 0.349 channels for X and 0.383 channels for Y. The detector resolution is then calculated by deconvoluting the beam width (0.726mm at half depth) out, which gives a FWHM resolution of 0.459mm in X and 0.534mm in Y. The practical readout spatial resolution of the detector is of course convolved with the digital resolution of the readout system $W/\sqrt{12}$, where W is the readout pitch, leading to FWHM values of 0.938mm and 0.866mm for X and Y respectively.

A 0.5mm collimated slit beam was then scanned across the entire length of the detector, in both dimensions, in 1mm steps. Figure 10 shows how the measured position and sigma, the standard deviation, vary across the detector length through the profile along Y=25. Figure 11 shows this variation for the Y data along X=25. The oscillatory behaviour of the sigma in X is due to Moire interference between the 1mm positions of the collimated beam and the 1.2mm pixel spacing. The large sigma in Y at the ends of the scans are thought to be due to asymmetric event collection.

Flooding the entire area of the detector with x-rays highlights any non-uniformities present in both the electronics and the detector. The discriminator thresholds were adjusted manually in order to minimise electronic non-linearities. Figure 12 shows two profiles, across X=25 and Y=25, from a flood of the counter once the adjustment has been made. The RMS error of the mean value gives a value of 3.2% in X and 6.2% in Y if the last point is ignored. This outlier is thought to be due to the detection of events outside the active area, as proved when the beam is tightly collimated, but why this behaviour is not seen at the other end is not clear.

The rate performance of the system was measured by using a range of aluminium attenuating sheets to adjust the source rate. As figure 13 shows the global system will acquire data at up to one million counts per second. The global dead time (counter, encoder and DAE acquisition system) is ~200ns. No tests have been carried out to characterise the rate capability of the detector and encoder separately. The ISIS DAE electronics is limited to a rate of the order observed (a new version is being made which will double this performance). The potential of the counting system is almost certainly higher. In particular, the parallel nature (48 channels) of the triggering system means that the 200ns occupancy of an x-ray pulse does not, in principle, determine the trigger rate of the global system, which could be of the order of a factor of five faster. This would permit rates of greater than 10MHz (provided the data capture system can handle this event rate).

The poor signal to noise ratio in the Y channels tends to lead to some degree of corruption and loss of events and so reduce the encoder efficiency below 100%, as well as degrading the uniformity of response in this dimension.

4. Discussion

The results presented above from the prototype 2-D GMSD show that a high rate (>MHz) 2-D x-ray detector design with sub-millimetre spatial resolution can be based on the principles described. The target design aims at an active area of 200mm x 200mm with a plate anode pitch of 0.5mm and a Y wire plane of the same pitch. In this case the digital contribution to the resolution (0.34mm FWHM) would scarcely increase the intrinsic resolution as measured in figures 8 and 9 (≈0.5mm FWHM). Further work is required to define the upper rate limit of the encoding system and the connection to an adequately speedy data capture system.

It is anticipated that useful improvements in the signal to noise ratio in the Y channels and improved alignment methods for the channel sensitivities can be achieved so aiming at a differential linearity in the region of 2%.

Funding has been secured, via the centre for instrumentation, to build a 200 by 200mm version of this detector. This detector will be specifically designed to explore the use of the existing RAPID readout system at the SRS at Daresbury [8]. Initial testing will be carried out using x-rays with the gas filling at atmospheric pressure, but a similar detector mounted in an atmosphere of pressurised ^{3}He would be suitable for neutron imaging.

References

1. J.E.Bateman, G.E.Derbyshire, D.M.Duxbury, A.S.Marsh, N.J.Rhodes, E.M.Schooneveld, E.J.Spill and R.Stephenson RAL-TR-2004-028

2. C.Cork, D.Fehr, R Hamlin, W.Vernon, N.Huu Xuong and C.Perez-Mendez, J. App. Cryst. (1973) 7, 319

3. M.E.Andianova, D.M.Kheiker, A.N.Popov, V.I.Simonov, Yu.S.Anisimov, S.P. Chernenko, A.B.Ivanov, S.A.Movchan, V.D.Peshekhonov and Yu.V.Zanevsky, J. App. Cryst. (1982) 15, 626

4. R.Kahn, R.Fourme, R.Bosshard and V.Saintagne, Nucl. Instr. and Method A246 (1986) 596

5. R.P.Phizackerley, C.W.Cork and E.A.Merritt, Nucl. Instr. and Method A246 (1986) 579

6. J.E. Bateman, J.F. Connolly, R. Stephenson, C.J. Bryant, A.D. Lincoln, P.A. Tucker and S. Swanton, Nucl. Instr. and Method A 259 (1987) 506

7. G.C. Smith, B. Yu, J. Fischer, V. Radeka and J.A. Harder, Nucl. Instr. and Method A 323 (1992) 78

8. R.A. Lewis, W.I. Helsby, A.O. Jones, C.J. Hall, B. Parker, J. Sheldon, P. Clifford, M. Hillen, I. Sumner, N.S. Fore, R.W.M. Jones and K.M. Roberts, Nucl. Instr. and Method A 392 (1997) 32

9. F. Angelini, R. Bellazini, A. Brez, M.M. Massai, G. Spandre and M.R. Torquati, Nucl. Instr. and Method A 283 (1989) 755

10. F. Angelini, R. Bellazini, L. Bosisio, A. Brez, M.M. Massai, A. Perret, G. Spandre and M.R. Torquati, Nucl. Instr. and Method A 323 (1992) 229

11. H. Takahashi, K. Yokoi, K. Yano, D. Fukuda, M. Nakazawa and K. Hasegawa, Nucl. Instr. and Method A 471 (2001) 120

12. S.F. Biagi, J. Bordas, D. Duxbury, E. Gabathuler and T. Jones, Nucl. Instr. and Method A 336 (1995) 76

13. C. Budtz-Jorgensen, Rev. Sci. Instrum. 63 (1) (1992) 648

14. J.E. Bateman, J.F. Connolly, G.E. Derbyshire, D.M. Duxbury, J. Lipp, J.A. Mir, J.E. Simmons, E.J. Spill, R. Stephenson, B.R. Dobson, R.C. Farrow, W.I. Helsby, R. Mutikainen and I. Suni, Nucl. Instr. and Method A 477 (2002) 340

15. J.E. Bateman, J.F. Connolly, G.E. Derbyshire, A.S. Marsh, R. Stephenson, J.E. Simmons, E.J. Spill, B.R. Dobson, R.C. Farrow, W.I. Helsby, R. Mutikainen and I. Suni, RAL-TR-1998-073

16. J.E. Bateman, N.J. Rhodes and R. Stephenson, Nucl. Instr. and Method A 477 (2002) 365

17. J.E. Bateman, N.J. Rhodes and R. Stephenson, RAL-TR-1998-024

18. J.E. Bateman, J.F. Connolly, R. Stephenson, M. Edwards and J.C. Thompson, Nucl. Instr. and Method A 348 (1994) 372

19. Final status report of the RD28 collaboration, CERN-LHCC-96-018

20. A.D. Smith, J.E. Bateman, G.E. Derbyshire, D.M. Duxbury, J. Lipp, E.J. Spill and R. Stephenson, Nucl. Instr. and Method A 467-468 (2001) 1136

21. M.W. Johnson, S.P. Quinton, RAL-NDRP-8504

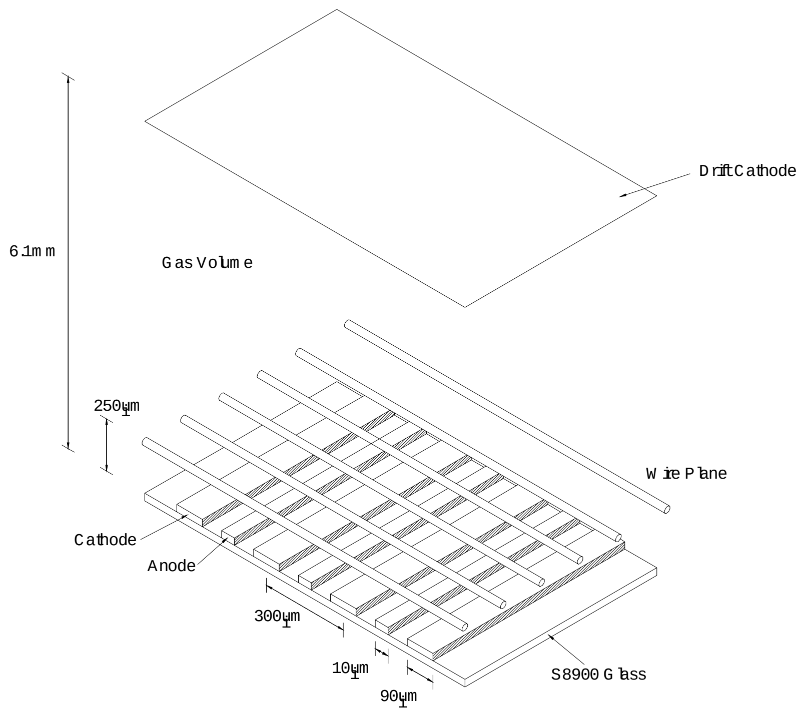

Figure 1: Schematic diagram of the detector geometry

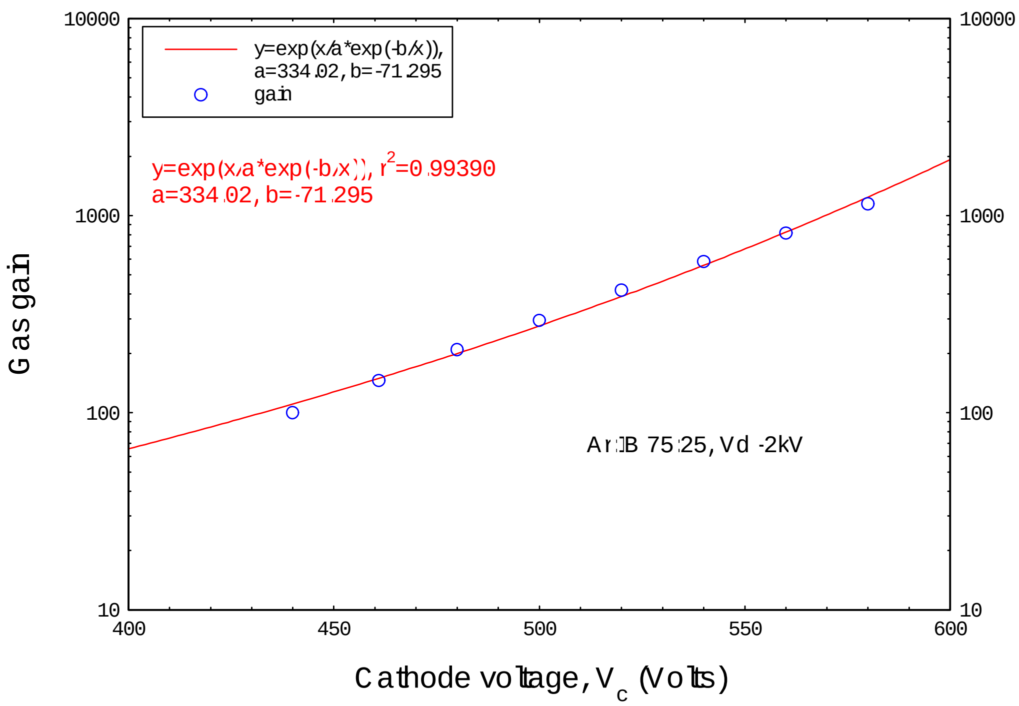

Figure 2: Gain variation of the GMSD as a function of cathode voltage

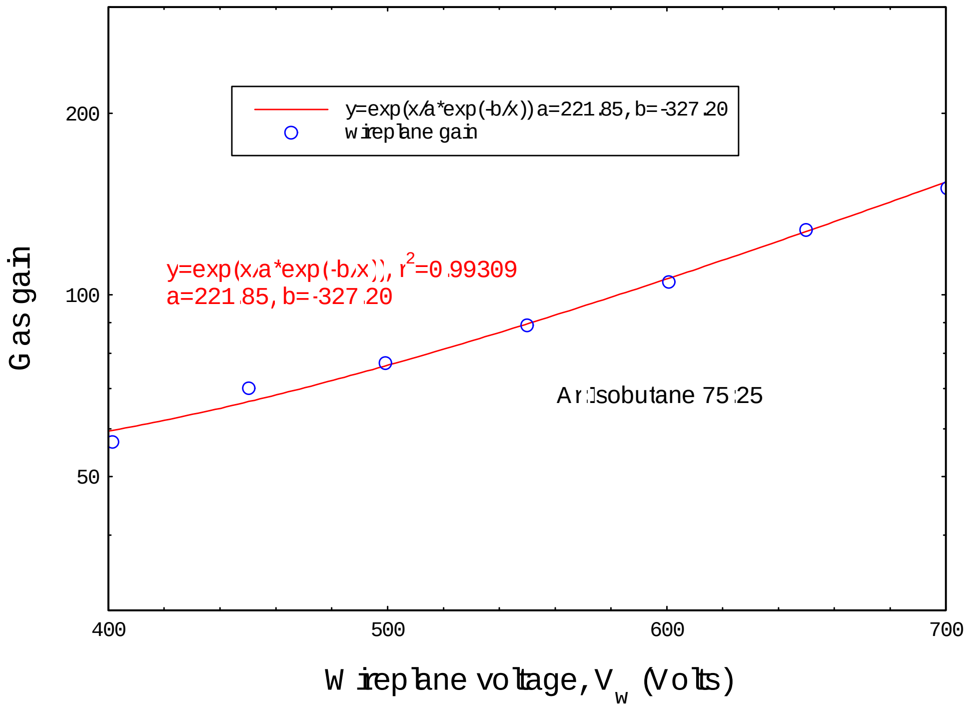

Figure 3: Gain variation of the GMSD as a function of wire-plane voltage

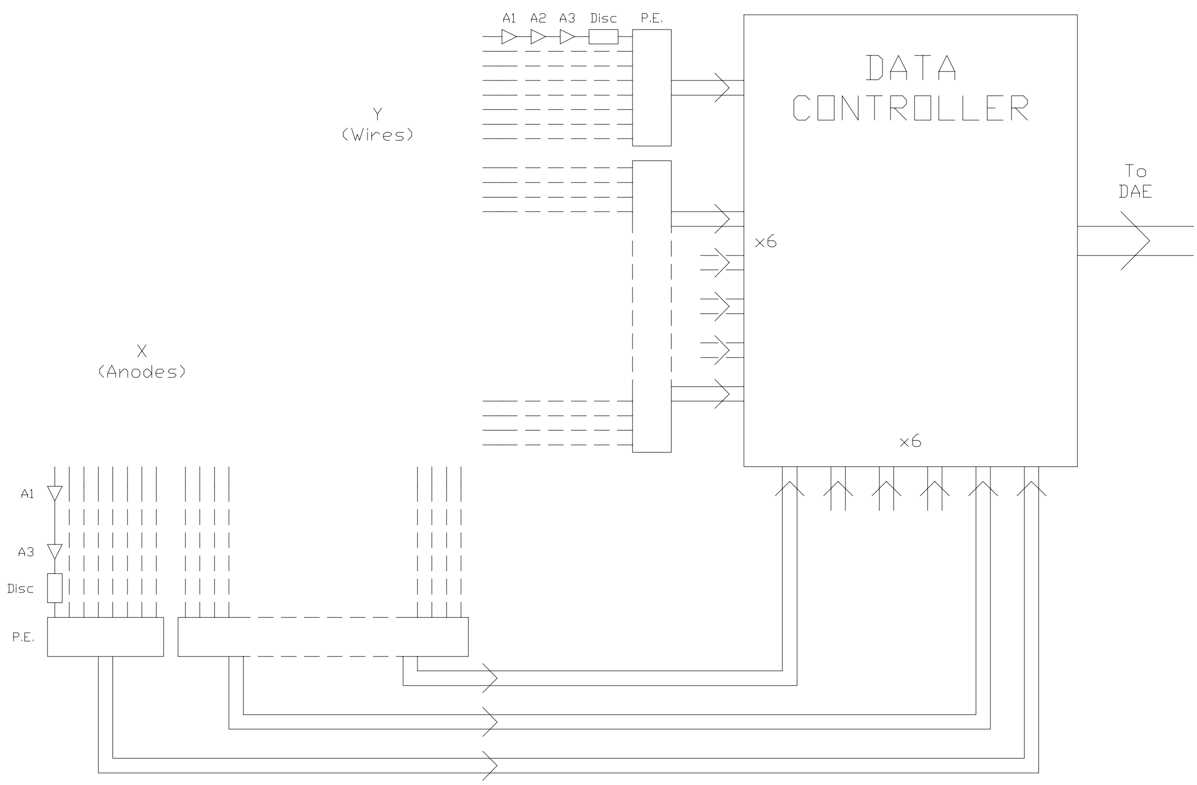

Figure 4: Schematic diagram of the electronic readout. Where A1 is the 16 channel preamplifier; A2 is the shaping amplifier; A3 is the NIM postamplifier; Disc is the NIM discriminator and PE is the primary encoder

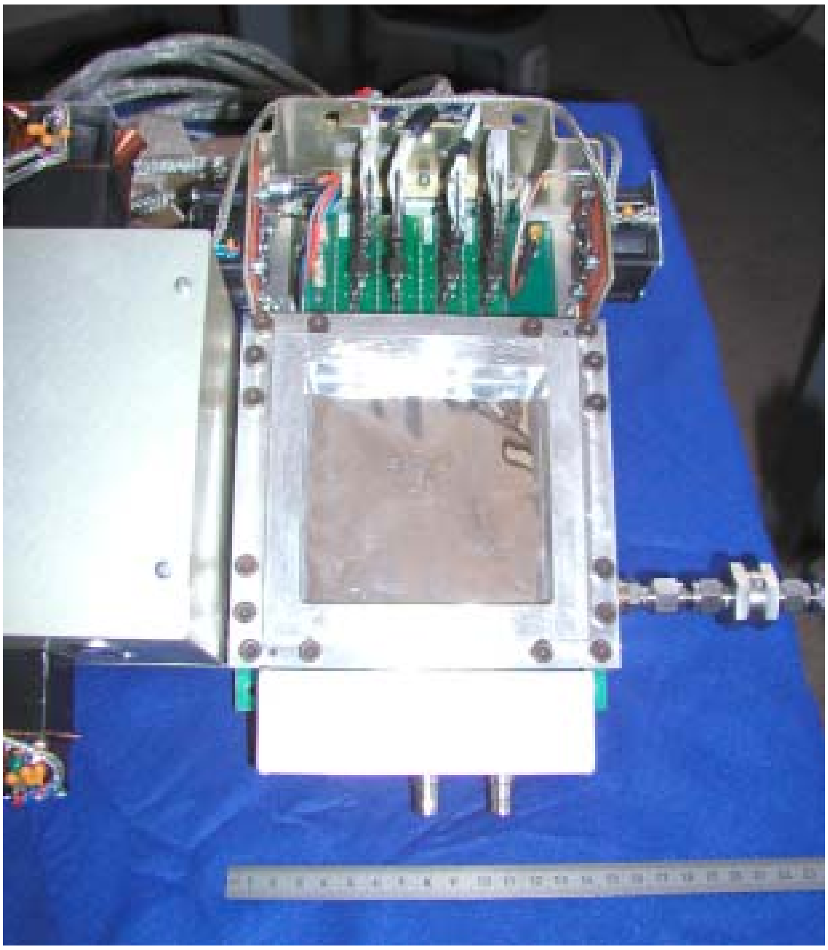

Figure 5: Photograph of the fully instrumented detector

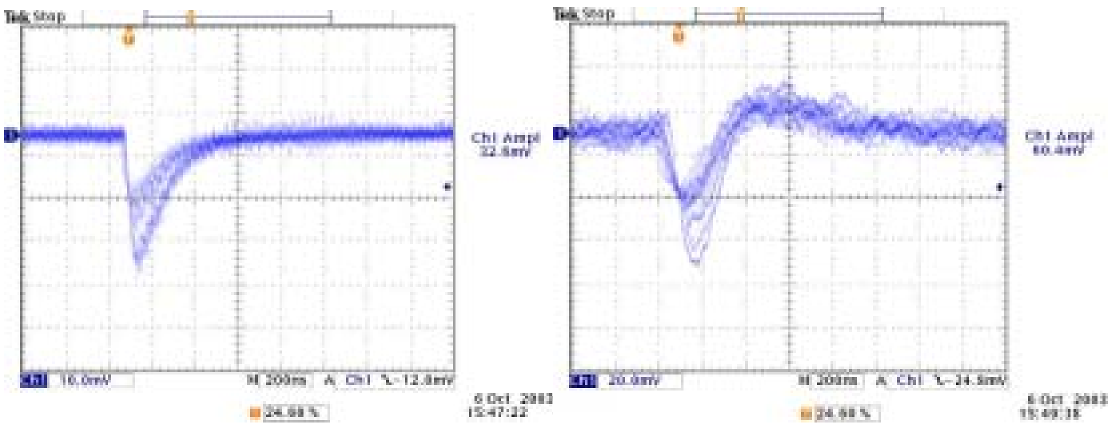

Figure 6: Typical pulses from the GMSD preamp (left) and wireplane preamp/shaper (right) for ^{55}Fe x-rays for single channels.

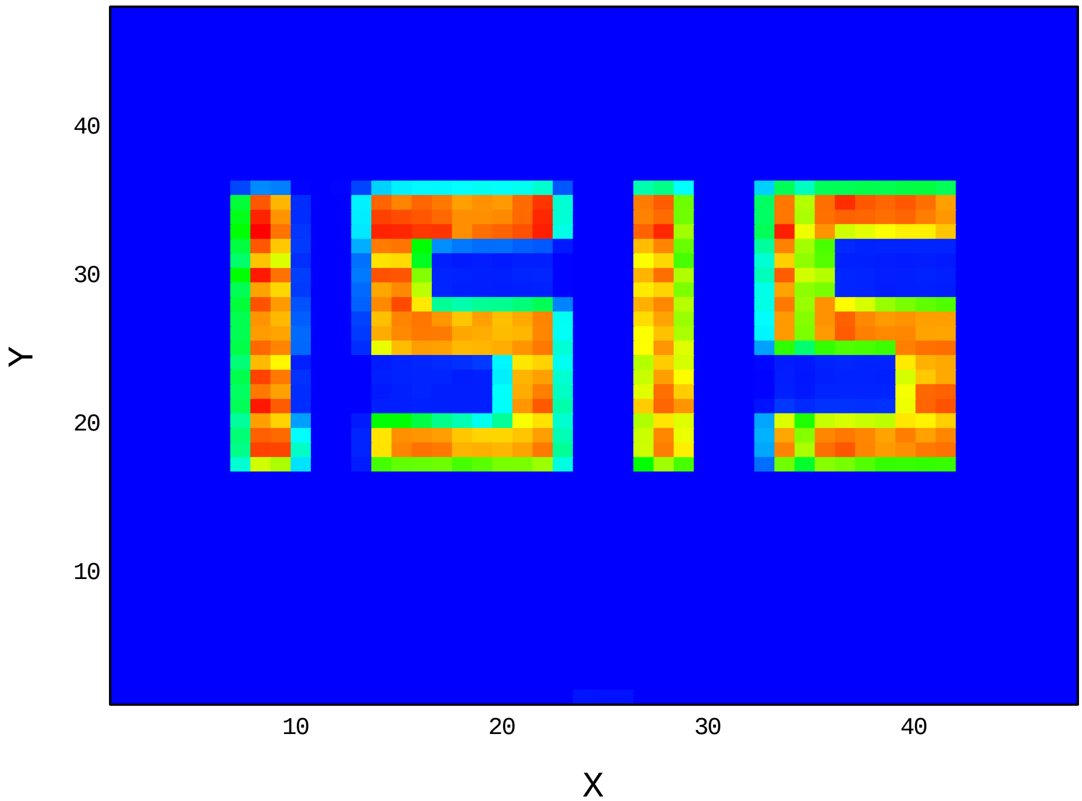

Figure 7: Image of copper 'ISIS' mask taken with the 2-D detector and ^{55}Fe x-rays

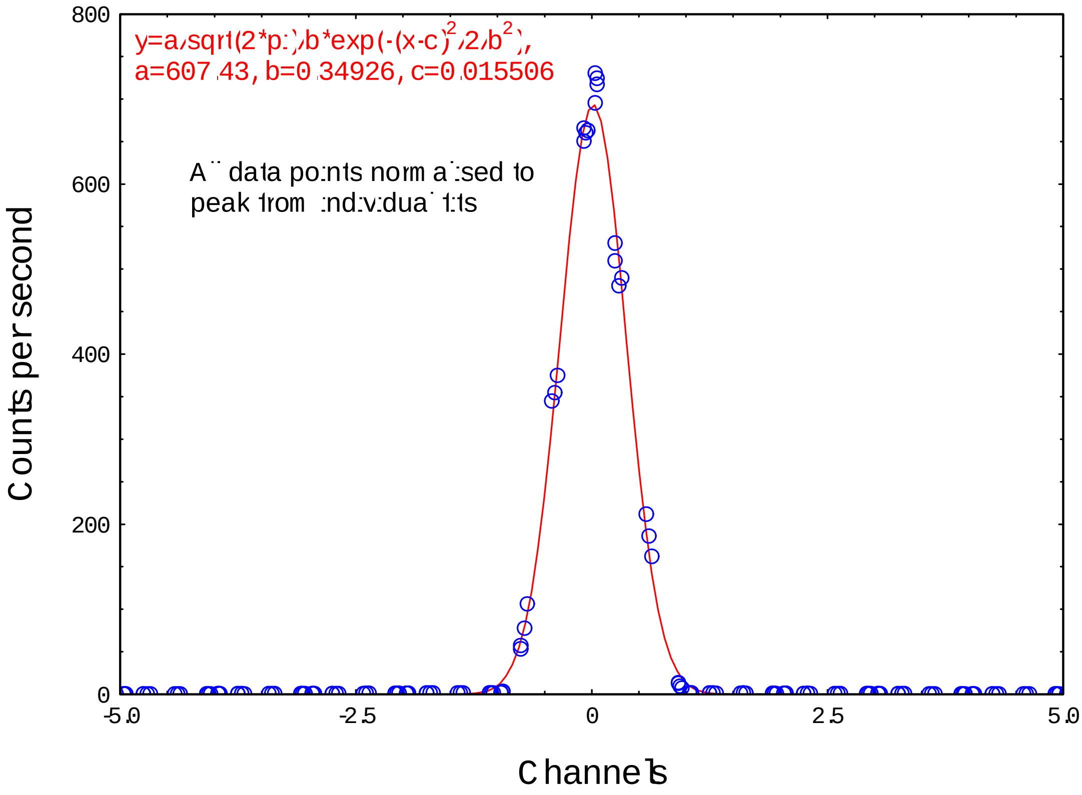

Figure 8: Intrinsic detector spatial resolution using interpolated readouts for X

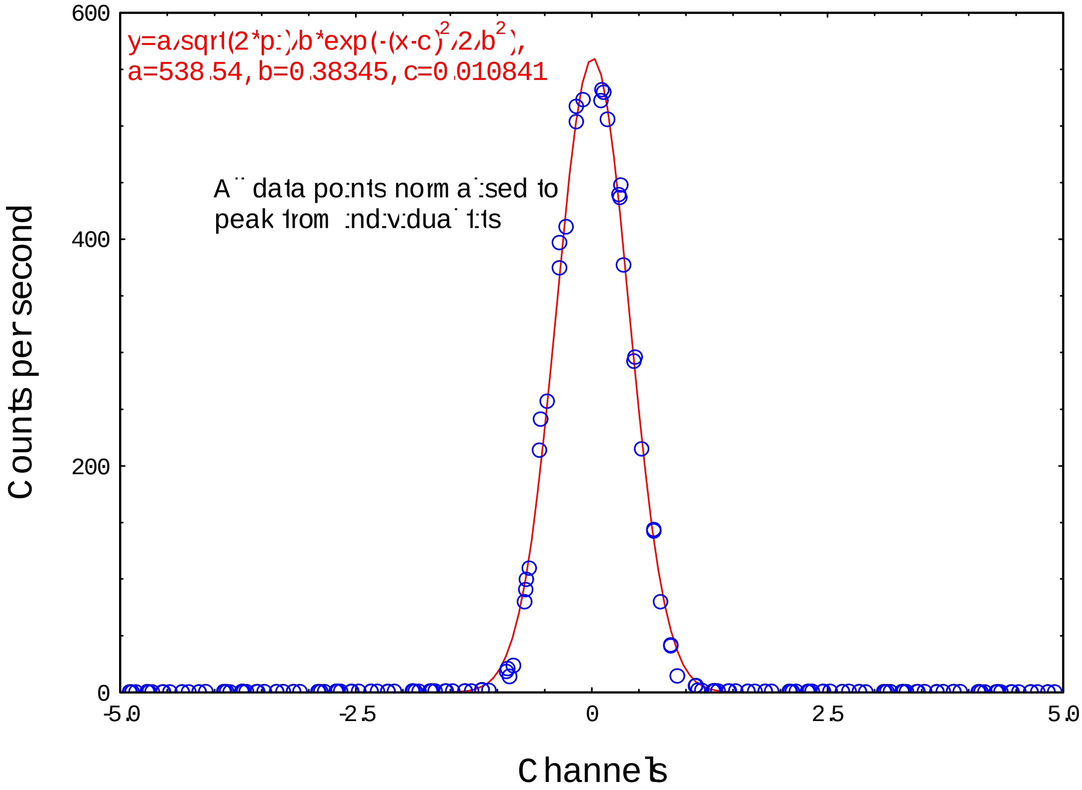

Figure 9: Intrinsic detector spatial resolution using interpolated readouts for Y

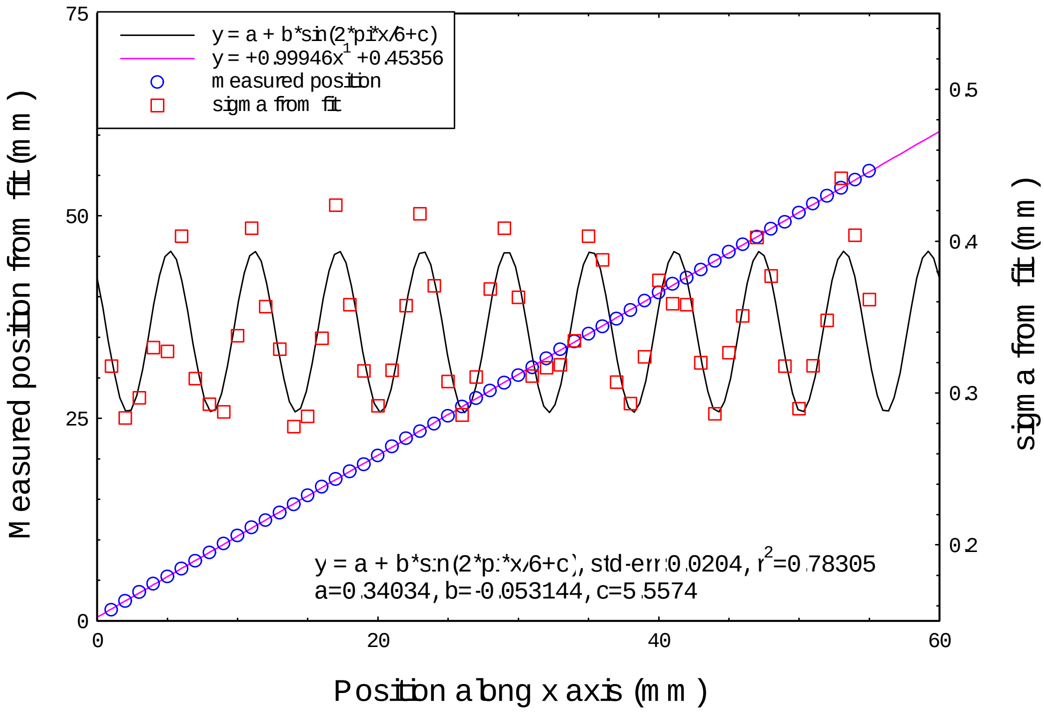

Figure 10: Variation of spatial resolution (sigma) and measured beam position as source moved along full length of detector

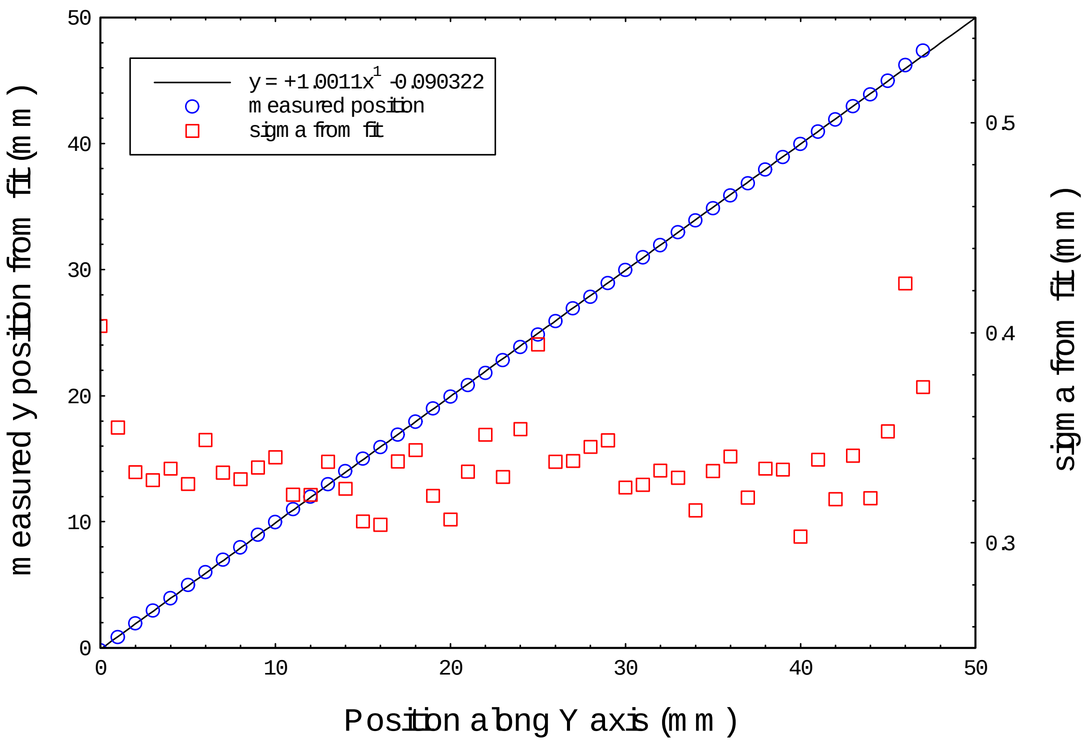

Figure 11: Variation of spatial resolution (sigma) and measured beam position as source moved along full height of detector

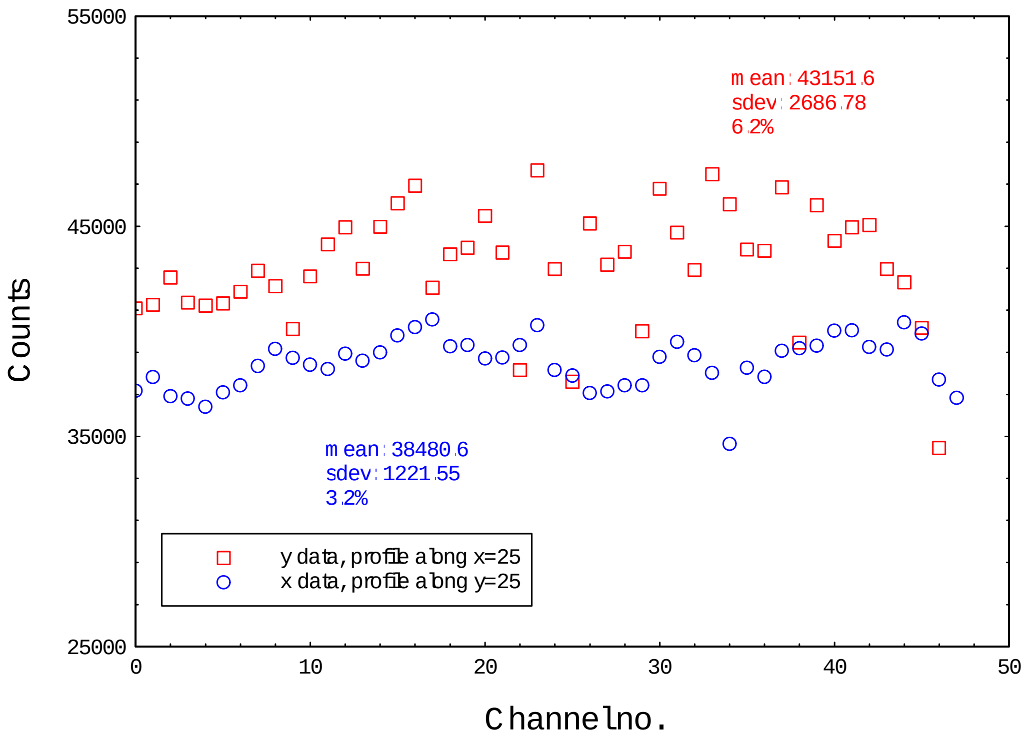

Figure 12: Uniformity of response along lines x=25 and y=25 for flood of entire detector area

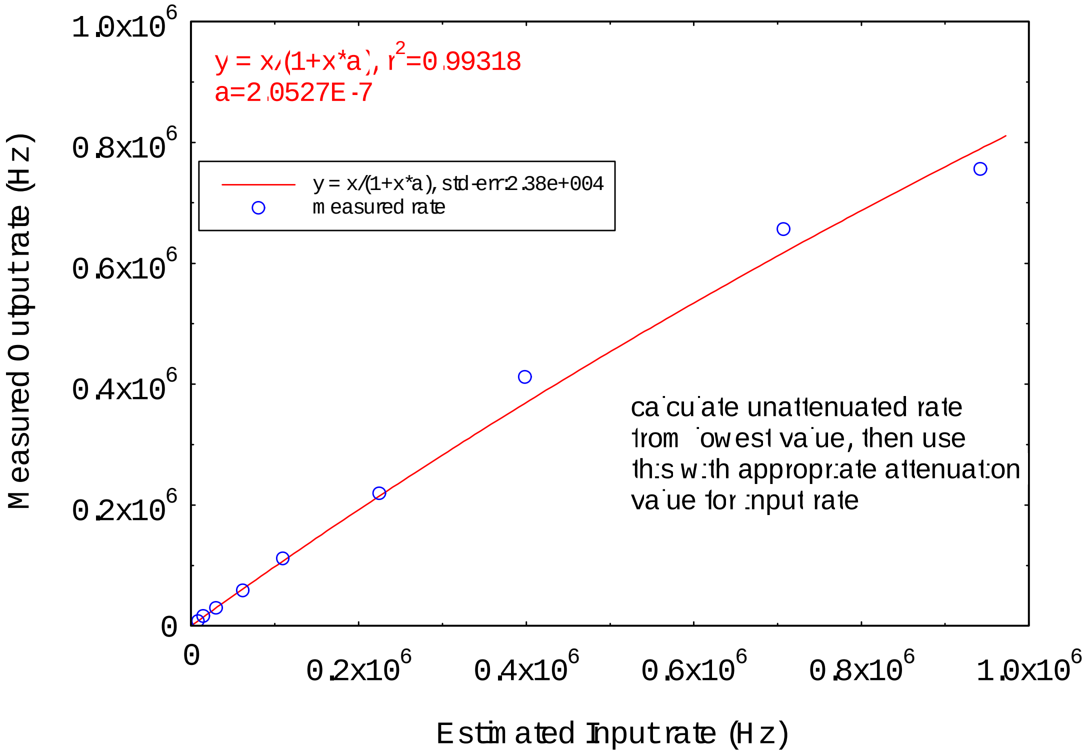

Figure 13: Rate performance of the detector with global flood.

Appendix 1: Description of the combining and encoding module serial number DEG 510

A block diagram of this unit is shown in the figure below. The eight inputs from the discriminator are fed into NIM to TTL converters. The converted signal is then fed into a Latch chip and an OR Gate. The O/P from the OR gate is then fed into another OR gate along with O/P's from the other seven OR gates (part of circuit enclosed by box is repeated seven times). A signal out of the second OR gate is generated if any one or more of the 64 I/P's (8×8) are present. This signal from the OR gate starts off monostable 1. The width of this pulse determines the total width of the latch signal and the delay after the latch. An O/P from monostable 1 triggers monostable 2, the width of which is the amount of time that the data is held by the latch for the rest of the circuitry to work. This is effectively the coincidence time window and is set at 200ns. The longer this pulse the longer the data is on the output for. O/P from monostable 1 also triggers monostable 3, the O/P of which is used to form the data ready pulse. The data that is held by the latch is fed into an EPROM (type AM26C512). This gives out a six bit address depending on which I/P was present. The EPROM can be programmed to accept various hit patterns. For the results presented above the EPROM has been programmed to accept double hits as well as single channel hits. For the double hits, that is events which fire two adjacent channels, the hit is arbitrarily assigned to the address with the least significant bit.

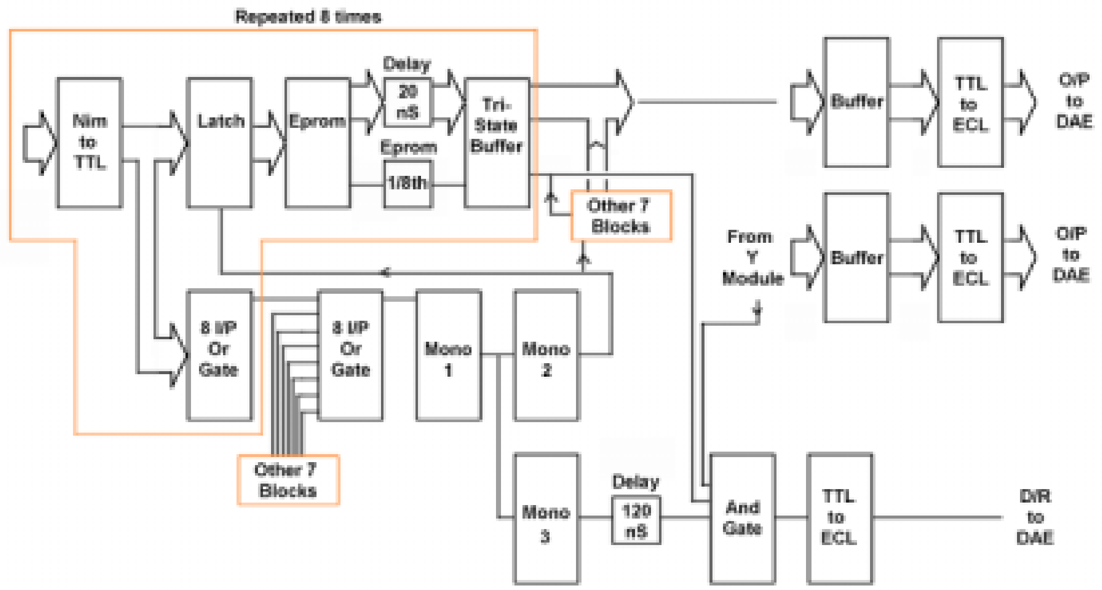

A comparison was made between the EPROMS programmed to accept just single hits and the EPROMS programmed to accept single and double hits. As expected, with the EPROMS programmed to accept double as well as single events, 21% more events were accepted. For the data presented in this paper the EPROMS have been programmed to accept single and double hits. If there is no valid I/P combination then the O/P is 000000. The EPROM also generates a data ready signal, which is fed along with the data into some delay lines. The EPROM also generates a chip enable signal, which along with the signals from the other seven circuits is fed into another EPROM. This EPROM switches the TRISTATE buffer O/P's either on or into tri-state. Only one of the eight Tri-states can be on at any one time. The data from the tri-state is then converted into ECL logic. The EPROM D/R signal, the monostable D/R signal and the D/R signal from the other module are all ANDED together and the resulting pulse is converted to ECL. At the same time, data from the Y module is also converted into ECL. For a valid data ready pulse to occur then the following must be present:

a) Monostable 3 output must be present, indicating that one or more of the 64 I/P channels had a signal.

b) EPROM D/R must be present indicating that the combination of input pulses was valid. In the case at the moment this is set to be either a single channel or two adjacent channels.

c) Data ready from Y module must be present, indicating that the Y module has had an event that also has met a and b criteria's.

The cycle time of the circuit has been measured to be 300ns.